http://www.aimspress.com/journal/Materials

Research article

Ductile fracture toughness of Al 5754-H111 alloy using essential work of fracture method

Mohammed Y. Abdellah[1,2,*], Nouby M. Ghazaly[1], Al-Shimaa H. Kamal[1], Abo-El Hagag A. Seleem[3] and G. T. Abdel-Jaber[1,4]

[1] Mechanical Engineering Department, Faculty of Engineering, South Valley University, Qena, 83523, Egypt

[2] Mechanical Engineering Department, College of Engineering and Islamic Architecture, Umm Al-Qura University Makkah, KSA

[3] Sun Miser Petroleum Company, Egypt

[4] New Assiut university of Technology (NATU), Assiut, Egypt

* Correspondence: Email: mohamed_abdalla@eng.svu.edu.eg.

Abstract: The aluminium alloy 5754 H-111 is a high-strength alloy with a remarkable corrosion resistance, particularly to seawater. It is widely used in the aerospace, marine, and automotive industries. In this work, the influence of fracture toughness methods applied to two thin aluminium sheets with different thicknesses (1.8 mm and 5 mm) was analysed. The first method was the essential work of fracture (EWF) method. It was applied at room temperature at a deformation rate of 1 mm/min with a double-edge notched tensile specimen (DENT) to measure the fracture toughness (w_e) of a material with ductile damage based on the stored energy of the body. The second method was a compact tensile test (CT) to determine the linear elastic fracture toughness. For the EWF, DENTs of 4, 6, 10, 12, and 14 mm were used in the centre section. The EWF values were 273 kJ/m^2 and 63 kJ/m^2 for the aluminium sheets with thicknesses of 5 mm and 1.8 mm, respectively. The surface energies J_{IC} determined using CT were 34.5 kJ/m^2 and 10.6 kJ/m^2, respectively, for these sheets. These values are highly similar. Furthermore, the percentage errors of the elastic EWF were 5.8% and 8.4%, respectively, for the two thicknesses. The fractures were of the stress types in which the pits and voids grow in conjunction. In addition, both deep and isolated large dimples were well distributed in the aluminium, which is the main ductile deformation concept.

Abbreviations: W_f: Total strain energy attributed to fracture; G_{Ic}: Surface release energy or critical mode I fracture toughness; J_{Ic}: Critical mode I fracture toughness; K_{Ic}: Fracture toughness; P_Q: Applied load; w_e: Essential work of fracture in the elastic zone; β_p: Geometric shape factors related to the plastic zone during tearing after necking; β_y: Geometric shape factors related to the plastic zone during ligament yielding; $a_\circ$: Pre-crack length; L: Ligament length; t: Thickness of the specimen; w: Sample width; w_p: Non-essential work of the fracture; W_p: Work of the tearing and necking of the plastic zone; W_{pp}: Relative plastic energy in tearing and necking; Wpy: Relative energy in plastic and yielding of ligament length; W_y: Elastic energy of the elastic and yielding ligament length; w_y: Essential work of fracture in the elastic zone; β: Plasticity shape factor; βwp: Slope of linear fitting regression; $\delta_\circ$: 0.2% offset displacement; $f\left(\frac{a}{w}\right)$: Correction factor

1. Introduction

In recent years, aluminium alloys have been sought in the ground vehicle industry because of their special properties, namely, a combination of strength, fatigue resistance, formability, and corrosion resistance. This helped classify these as special metals. Magnesium yields 5754 H-111 aluminium alloys. Their strength originates from the solid-solution strengthening. Chromium, manganese, and zirconium are added to control the grain and subgrain structures and increase the strength of the alloys. The H111 designation for the condition differs from the O condition in that semi-finished products supplied in this condition are rolled after annealing to improve their dimensional properties such as flatness [1,2].

It is important to understand the fracture mechanisms to prevent in-service failures owing to design and usage problems. Fracture mechanics are dependent on crack-like material defects regardless of their origin. It is a gradual as well as temporally and spatially inhomogeneous process that begins with the initiation of a crack, propagates, and eventually causes the fracture or coalescence of cracks. This occurs when stresses do not exceed the yield stress. The critical stress concentration for fracture is still in the range of linear elastic fracture mechanics and is an inherent material property, K_{IC} [3]. Toughness is an important parameter for measuring the capability of a material to absorb energy before failure. This energy is considered to represent a large plastic deformation before separation, which is the main difference between brittle and ductile fractures.

The essential work of fracture (EWF) approach [4] is effective for dividing the total energy expended in the FPZ into two components: the EWF w_e and non-EWF w_p. The crack propagation resistance is represented by the EWF, w_e. The critical fracture energy (G$_{IC}$) differs from the J-integral and represents the actual crack-propagation resistance after the initiation of a fracture.

Shinde et al. [5] used a modified one-sided notched specimen design to measure thin 6061-T6 alloy aluminium plates. The modified design reduced buckling of the specimen. It was observed that the fracture toughness of the thin 6061-T6 aluminium alloy plates was higher than the plane load toughness. However, a linear finite element model was used to calculate the stress field distribution.

Tippeswamy [6] conducted an experiment using aluminium 6082-T6 in accordance with ASTM standards. The specimens were tested by varying the notch length within a specified constraint. The

experimental results showed that the notch length significantly affected the size of the plastic zone at the end of the cut. Furthermore, the rates of fracture formation and propagation varied depending on the notch length of each specimen.

Pardoen et al. [7] investigated the influence of sheet thickness on the fracture strength of a thin sheet of the aluminium alloy 6082-o with a thickness of 1–6 mm for the final separation using the EWF and J-integral methods in a tensile test (double-edge notched tensile specimen (DENT)). Their study aimed to determine the relationship between these two strategies. The EWF is a measure of the fracture initiation resistance. Go when there are few variations in GC.

Using numerical simulations, Moiseenko et al. [8] analysed hybrid discrete-continuous cellular automata that enable the calculation of the local moments of force and the simulation of the dissipation of torsional energy. This resulted in the development of new defect structures. The simulations included the calculation of thermal expansion with the simultaneous build-up of thermal stresses and initiation of microrotation. This allowed for the assessment of local entropy and tracking of crystal defect evolution from the onset to storage. The mechanical behaviours of materials subjected to thermally-induced twinning or phase transitions were simulated, and the algorithms were explained.

Balokhonov et al. [9] presented a numerical analysis of the microstructural influences on the deformation and fracture of friction stir welds in aluminium alloys. The mechanical response of individual grains was simulated using an elastic–plastic formulation of the problem that considers isotropic strain hardening including the Hall–Petch effect, and a fracture model that permits crack initiation and growth in the regions of the maximum equivalent plastic strain. The strength of welded materials has been shown to influence the plastic strain and fracture localisation.

Balokhonov et al. [10] investigated the localisation of plastic deformation and fractures in a porous coated material. The numerical simulations were performed using the finite-difference method. The presence of localised tensile zones around the pores and at the interface between the coating and substrate (both in tension and compression of the coated material) was demonstrated to be the cause of the unique deformation and fracture characteristics of the composite studied. The relationship between the crack propagation in the coating and the inhomogeneous plastic flow in the steel substrate was investigated.

A thin aluminium strip was measured by Abdellah [11] using the EWF. A simple finite-element numerical model was constructed to predict the EWF parameters. Although the sample was measured in millimetres, the experimental results and proposed model agreed considerably. The concept of different energy zones around the fracture tip was first introduced by Broberg [12]. The fracture process zone (FPZ) and outer plastic zone are two subdivisions of the crack tip generated by Broberg. Two new surfaces were generated using energy from the FPZ. The FPZ is not affected by the loading conditions or stress at the fracture tip. The fracture length, load, shape, and stress state affect the outer plastic zone. Cotterell and Reddel first proposed the central thesis on the fracture concept in 1976 [4]. Cotterell and Reddel used the Broberg notion of energy expended in an independent autonomous end zone (sheet). In linear elastic fracture mechanics, the plastic zone around the crack tip is assumed to be marginal.

Korsunsky and Kyungmok [13] investigated the feasibility of quantifying the crucial work in ductile cracking using single tensile tests on dog-bone specimens without notches. They used different types of heat-treatable aluminium alloys. The obtained results were compared with those of a typical DENT. The authors concluded that a laser scanner could be used.

Most conventional methods [14–17] for determining fracture parameters such as G_{IC} or the stress intensity factor (SIF), K_{IC}, were developed considering isotropic materials when linear elastic fracture mechanics (LEFM) was originally developed.

Masuda et al. [17] used A7075-T6 compact tensile (CT) specimens of various thicknesses (1–21 mm) in fatigue crack growth studies. As the thickness decreases, the radius of curvature of the leading edge of the fatigue crack increases. The extent of the lateral plastic contraction (indentation depth d) at the crack tip during fatigue loading was estimated quantitatively using the three-dimensional elastoplastic finite element method. The results of the experiment are as follows. The rate of fatigue crack growth da/dN at a constant K increased with an increase in t from 1 to 11 mm in the range where $K \geq 5$ MPa$\sqrt{m}$. Between t = 11 and 21 mm, da/dN remained constant. Meanwhile, in the range where K is less than 5 MPa$\sqrt{m}$. A J-R curve (or D–R curve) is a plot of the resistance to stable crack extension measured as J (or R-d) plotted against ductile crack extension (generally considered as Dap, the measured physical crack extension). However, in many cases, only estimates of this crack extension are available. ASTM E1820 [18] was developed for measuring the elastic–plastic initiation toughness, J_{IC}, and J-R curves or the corresponding dIc and d-R curves under plane-strain conditions. However, in [19], it was developed for evaluating the CTOD at the onset of cleavage, dc. In thin-walled materials with low constraints, the CTOA parameter is used to describe stable crack extension.

Complex crack configurations in finite plates pose a significant challenge for SIF calculations. Byskov [20] proposed a thorough numerical FEM to solve the above problems by focusing on specific cracked elements, Here, the stiffness matrix is connected to the crack elements. To determine the K-R curves according to ASTM E1820, Lu and Wang [21] tested C(T) and M(T) specimens over a range of thicknesses (plane stress and plane strain). A novel method was presented for determining the CTOA using the K-R test data. Considering the effective performance of the ASTM E1820 test, Di et al. [22] recommended the use of a modified C(T) specimen to evaluate the CTOA of X80 pipeline steel. Finite element analysis (FEA) was used to predict the failure of the C(T) and M(T) specimens based on the CTOA fracture criteria.

As mentioned in the previous paragraph, many researchers have studied the fracture toughness of the aluminium alloy 5754-H111 (also known as Al-Mg) under ductile damage using linear elastic fracture mechanics. Therefore, this study focuses on using other indirect methods with a simple technique to complete the description of the plastic behaviour of materials. The objectives of this work are as follows: (1) to establish that the EWF method is reasonable for measuring the fracture toughness in ductile damage energi J_{IC}, (2) to compare the results of standard compact tensile specimens with EWF, and (3) to investigate the fracture topography and failure modes in ductile damage.

The paper is structured as follows: In the first section, the EWF concepts are outlined. Then, the material and method are explained. In the third section, the results of the EWF and CT are illustrated and discussed. Finally, the comparison is limited to the applicability of the method.

2. Essential work of fracture method

2.1. Analytical model

The EWF method can be used to evaluate the fracture toughness of thin layers of materials. It has gained considerable popularity in recent years [5]. According to the EWF method, the total energy (W_f) required to fracture a notched specimen is divided into two parts: the essential work (W_e) used to generate new surfaces in the so-called fracture process zone and the non-essential work (W_p) used to plastically deform the area around the process zone. Therefore the specific work, W_f, can be expressed as the combination of the following two terms [11] (see Eqs 1–3):

$$W_f = \int_0^\delta p \; d\delta \tag{1}$$

$$W_f = W_e + W_p \tag{2}$$

$$W_f = W_e + \beta W_p \tag{3}$$

Figure 1 shows the EWF technique used to break the surfaces of typical DENT specimens. When the two plastic zones are formed at the crack touch, the ligament L yields completely under the maximum force applied to the specimen [23]. The curve between the load and displacement when the ligament fails completely owing to ductile cracks is shown in Figure 2 [11,24].
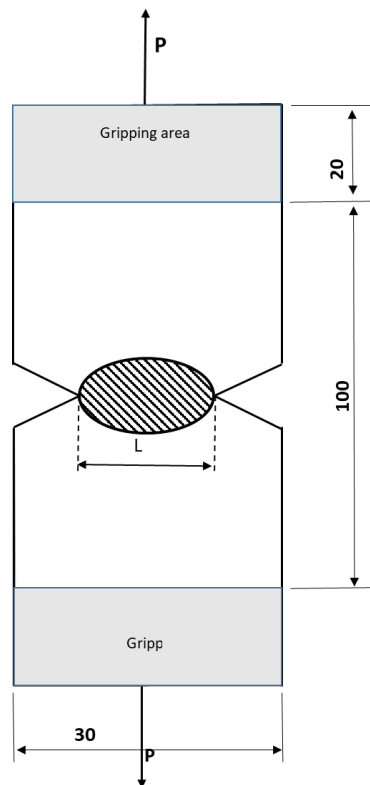
Figure 1. Double-edge notched specimen with a plastic zone [24,25].
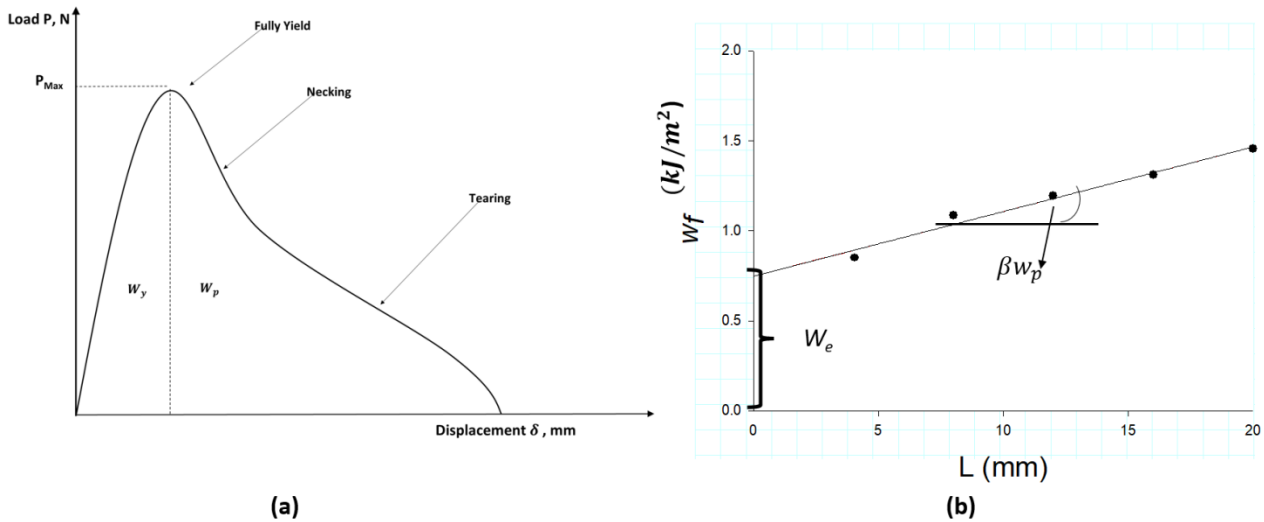
Figure 2. EWF data (a) load–displacement curve and (b) EWF fitting [25].

Here, W_p is the plastic deformation zone behind the fracture process zone, we is the instability of the crack tip, and we is the surface release work in the crack process zone. Furthermore, the failure displacement δ. For a given specimen thickness, the surface release depends on the ligament length L. The volume energy (L^2t) is proportional to the volume. It describes the plastic work (W_p). Equation 2 is divided by the ligament area, Lt, to obtain the following expression for energy:

$$w_f = \frac{W_f}{Lt} = w_e + \beta \, w_p L \tag{4}$$

where β is the plastic work per unit volume of the plastic deformation zone in front of the crack tip as w_p, the specific non-essential work of the fracture, and, the shape factor of the plastic deformation. The surface release energy is also necessary for the formation of the cracked surface. The relationship between w_f and the ligament length L is shown in Eq 4. It is a linear regression. The range of the ligament lengths for the effective EWF tests was the plastic work per unit volume of the plastic deformation zone before the crack tip. In addition, w_e considers the surface release energy required to initiate the crack surface formation. The relationship of w_f shown in Eq 4 is a linear regression relating it to the ligament length L. According to the "rule of thumb" of Cotterell and Reddel [4], the range of ligament lengths for the valid EWF tests is shown in Eq 5:

$$L_{\min} = (3 - 5)t < L < L_{\max} = \frac{W}{3} \tag{5}$$

The positive intercept at $L = 0$ corresponds to a specific EWF. The slope of the regression line was determined by linearly fitting the data with the non-EWF, wp (see Figure 2b). After a load is applied and the ligament yields completely, Eq 2 for a DENT specimen could be rewritten as follows:

$$W_f = W_y + W_{pp} \tag{6}$$

where W_y is the mechanical energy in the elastic zone and W_{pp} is the plastic energy used for constriction or subsequent tearing in the plastic zone (see Figure 2a). Using Eq 4, w_e can be divided

into two zones: the elastic zone of EWF Wey associated with crack initiation and plastic zone of EWF $Wepp$ associated with cracking prior to necking before the crack tip (see Eq 7):

$$w_e = Wey + Wepp \tag{7}$$

Eq 8 expresses the divisions of the slope:

$$\beta W_p = \beta y\, w_{py} + \beta p\, w_{pp} \tag{8}$$

where βy and βp are the geometric slope parameters associated with the plastic zone during ligament yielding and tearing after necking, respectively.

3. Experimental work

3.1. Material description

The commercial aluminium 5754-H111 alloy specimens were obtained from Egypt Alum. Co. The chemical composition of the A5754 -T alloy is presented in Table 1.

Table 1. Chemical composition of aluminium 5754-H111 [26].

Zn	Cu	Mn	Si	Fe	Mg	Cr	Ti	Al
0.2	0.1	0.5	0.4	0.4	2.6–3.6	0.3	0.15	Bal.

These substances significantly affect aluminium alloy 5754. These provide a remarkable corrosion resistance, particularly in the presence of seawater and industrially polluted atmospheres. It is a medium-strength alloy. In accordance with the symbol H111, the alloy was subjected to formative work-hardening. The aluminium alloy 5754-H111 is characterised by a high fatigue strength, good machinability, and good cold formability. The alloy belongs to the high-strength 5xxx series. Therefore, 5754-H111 is highly suitable for use in flooring, shipbuilding, and structures addressing chemicals and nuclear energy. It is also widely used in structural components and interior trims of automobiles [27,28]. The chemical components were determined using XRD (see Figure 3). It showed that the maximum dislocation density was achieved by the following factors:

Peak Angle: 78.24 °, FWHM: 0.3380 °, Scherrer Crystallite Size: 53.86 nm

Peak Angle: 65.1 °, FWHM: 0.2860 °, Scherrer Crystallite Size: 68.53 nm

Peak Angle: 44.74 °, FWHM: 0.2460 °, Scherrer Crystallite Size: 88.49 nm

Start: 5 °, End: 80 °, Step: 0.02 °, Speed: 2.5 °/min, Time/Step: 7.999999E-03 °, Wavelength: 1.54056 (Cu).

It was observed that this aluminium alloy has a larger amount of Mg (2.6–3.6). This makes it more brittle and vulnerable to environmental effects. Meanwhile, Mn and Si have relatively higher values and can precipitate during cracking action.
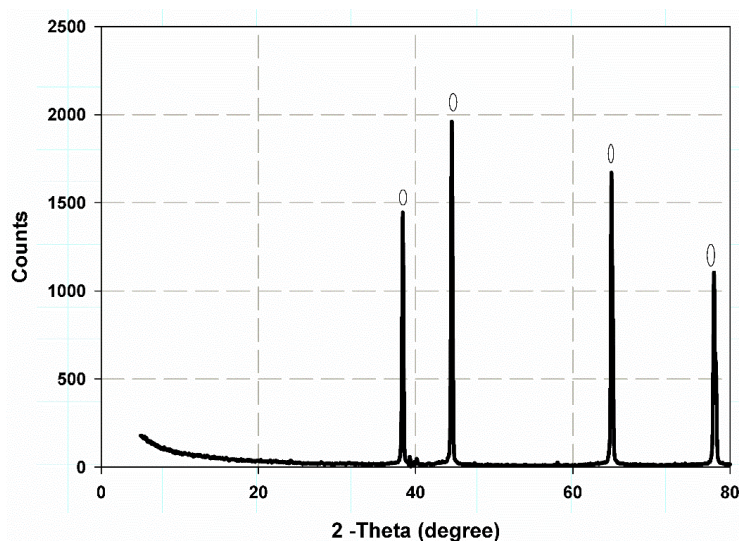
Figure 3. XRF for aluminium sheet A 5754.

3.2. Tension test (ductile damage)

A standard tensile test was performed according to ASTM E399-81 [29] to determine the following mechanical properties: tensile strength, elongation strength, Young's modulus, and percentage elongation. A standard rectangular tensile specimen with dimensions $90 \times 15 \times 10$ mm was used (Figure 4). The tests were conducted using a computer-controlled electromechanical universal testing machine (model WDW-100-Jinan Victory Instrument Co. Ltd., China) [30] with a loading capacity of 100 kN and controlled speed of 2 mm/min. To understand the ductile damage, the topography was investigated. The aim was to conduct these tests via SEM because the tensile test is a basic and standard test for investigating failure and damage.
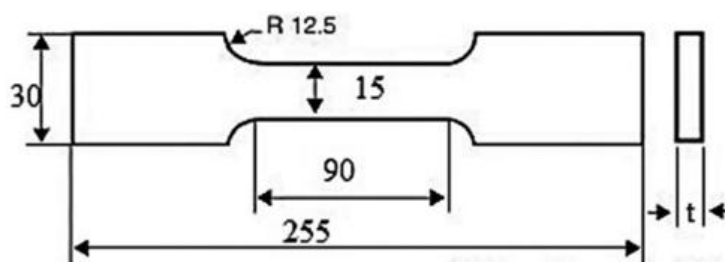
Figure 4. Tensile test sample.

3.3. Compact tension method

The specimens were subjected to an ASTM Standard D 5045 compliant fracture toughness test [31]. To obtain accurate results for the fracture toughness and plane strain fracture toughness K_{IC} (which indicates the resistance of a material to fracture), the crack resistance measurement should be stopped at the point of degradation. According to the measurements provided in ASTM D5045 [31], two compact tensile specimens were fabricated using a milling machine (see Figure 5). The specimens

were clamped between two sacrificial plates made of an identical material to prevent damage. Load holes were drilled using carbide drills. The initial crack was generated using a diamond blade with a thickness of 1 mm. The CT geometry is recommended because it enables planar loading with smaller specimen sizes than the other designs. The widths (W), thicknesses (t), and crack lengths (a) of the specimens are shown in Figure 4. The crack length a is 0.45–0.55 times W. The nominal value of the W / B ratio is two.

$$0.45 < a/W < 0.55 \tag{9}$$

Two thicknesses (t) of 1.8 mm and 5 mm were used. Both the specimens had a width of 60 mm and length of 65 mm, according to [32] (see Figure 5). These thicknesses were selected for porosities to study the effect of the Mg reaction during the test when oxygen penetrated the crack surface, from an available thin plate with a thickness of 1.8 mm and a larger thickness of 5 mm. It is also established that the fracture toughness depends on the thickness according to LEFM. Therefore, it would be effective to review this concept for the EWF technique [30]. The load corresponding to an apparent increase in the crack extension of 2.5% was determined by a certain deviation from the linear part of the record. K_{IC} was calculated from this load using equations established based on elastic stress analyses of specimens of the type described in the test methods. The generation of a sharp crack at the crack tip in a specimen sufficiently large to exhibit linear elastic behaviour is necessary to validate the evaluation of the K_{IC} value determined using these test methods.
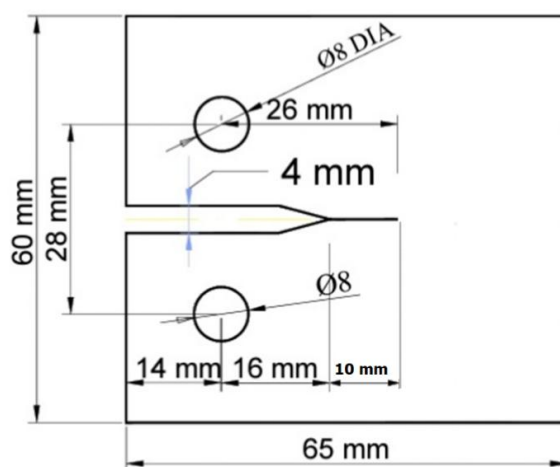
Figure 5. CT test specimen geometry [33].

3.4. Essential work of fracture test

A DENT was tested using a universal testing machine at a transverse speed of 2 mm/min at room temperature. The specimens had a length of five ligaments, as shown in Figure 1. The ligaments had lengths of 4, 6, 10, 12, and 14 mm. The specimen was cut with a CNC milling machine. The cracks were cut with a sharp blade of 1 mm thickness according to [34–37]. The load was applied on both sides of the specimen to complement failure, and the load and displacement were recorded. The number of specimens for each ligament was three. After complete failure

attained the mechanical energies, W_y and W_{pp} were calculated using Eqs 10 and 11 by integrating the resulting load–displacement curves as follows:

$$W_y = \int_0^{\delta_0} p \ d\delta \qquad (10)$$

$$W_{pp} = \int_{\delta_0}^{\delta} p \ d\delta \qquad (11)$$

where δ_0 and δ are the displacements at 0.02% offset and failure, respectively. p is the applied load. The obtained total energy W_f (measured using Eq 6) was plotted against the ligament length L. The displacement at fracture (δ) could be plotted against L according to [38].

4. Result and discussion

4.1. Tension test (ductile damage)

Figure 6 shows the stress–strain relationship obtained by the tensile test of the aluminium alloy 5754. It is observed that the stress was uniform, yield strength was 153.9, tensile strength was 265 MPa, and Young's modulus was 68 GPa. The percent elongation was 1.2, and the ductile fracture behaviour was characterised by a large plastic zone. The fracture investigation was performed by SEM image analysis. It was observed that in the case of the aluminium alloy before fracture, the alumina was distributed uniformly over the aluminium matrix, and no voids were observed (see Figure 7a). Although the case occurred after the fracture and deformation, it was observed that the deep pits were distributed over the matrix. This was owing to void coalescence. Moreover, MgO formed during the test. As the oxygen insert induced by the microcrach, these hard particles of MgO participated at the grain boundary of the lighter lines (see Figure 7b). The formation of these oxides rendered the alloy brittle, thereby resulting in microcracks. It was also observed that the higher strength was owing to the strong bonding between the alloying elements [39,40]. The results are summarised in Table 2.
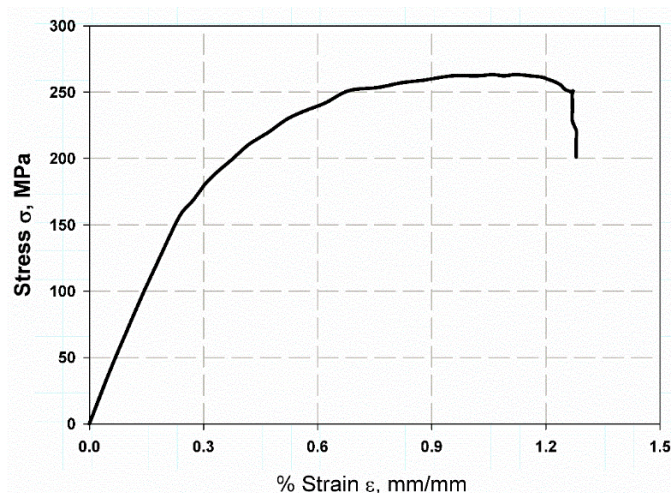
Figure 6. Stress and strain relationship for aluminium alloy.
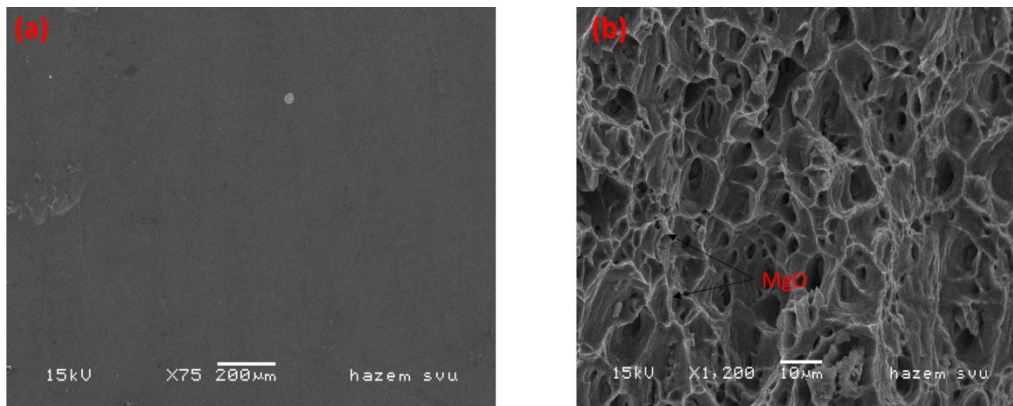
**Figure 7.** SEM image of fracture surface in tension.

Table 2. Mechanical properties of Al 5754-H111 alloy.

Yield strength (MPa)	Ultimate tensile strength (MPa)	Young's modulus (GPa)	% elongation
153.9	265	68	1.2

## 4.2. Essential work of fracture

Figure 8a,b shows the force–displacement curves obtained from the EWF measurement of the 5 mm and 1.8 mm aluminium DENT specimens at room temperature. The curves show a linear increase up to a certain point where an oscillation occurs indicating the flow range. These continue to increase until these attain the peak value (full flow). Then, ductile cracking and eventual failure occur. The load-displacement curves as a function of ligament length show similar geometries. The total energy W_f stored in the cracked specimen is represented by the area under the force-displacement curve. This area is measured using Eq 1. The internal work increases with an increase in the ligament length (middle part). This is owing to the increase in the amount of material to be deformed. The crack then propagates through the material as the resistance increases (the length of the fracture zone increases as the ligament length increases). A decrease in the ligament length implies an increase in the crack initiation length a_0. To obtain the elastic work of fracture W_y, the area under the linear intercept of the force–displacement curve was plotted. The total work W_f under the curve was then divided by the area of the ligament portion (Lt). Thereby, the relationship between the total work W_f with each ligament was poled as shown in Figure 9. The linear regression of the total work done per ligament area is shown in Figure 9a,b for the DENTs with thicknesses of 5 mm and 1.8 mm, respectively. It was observed that the w_e as the intersection point between the extension of the linear regression data with the yaxis was separated. It was 273 kJ/m^2 and 63 kJ/m^2 for the plates with thicknesses of 5 mm and 1.8 mm, respectively. This demonstrated that the EWF sensitively tested the thickness. The higher value is owing to the MgO formation caused by oxygen penetration into the crack during the crack propagation. The MgO particles were distributed over the crack surfaces for the 5 mm-thick plates [41]. These solid microscopic particles bridge the crack surfaces, thereby reducing the crack propagation or advancement. At a low thickness, the fracture toughness was relatively low at 63 kJ/m^2. This was owing to the thin crack surface having only a marginal amount of bridging by the crack. In addition, the Si would crack and thereby contribute to

the fracture [42]. The elastic EWF *Wey* was shown in Figure 10a,b. It was 36 kJ/m^2 and 11.5 kJ/m^2 for the thicknesses of 5 mm and 1.8 mm, respectively. The value for 5 mm is near the standard range of fracture toughness in the ASM standard [43], whereas the value for 1.8 mm is below the range. This can be attributed to the fact that the fracture toughness is sensitive to the thickness. Even at a small thickness, there was a larger amount of localised stress. The modes of failure were net tension as shown in Figure 11a,b for all the specimen with thicknesses of 5 mm and 1.8 mm, respectively.
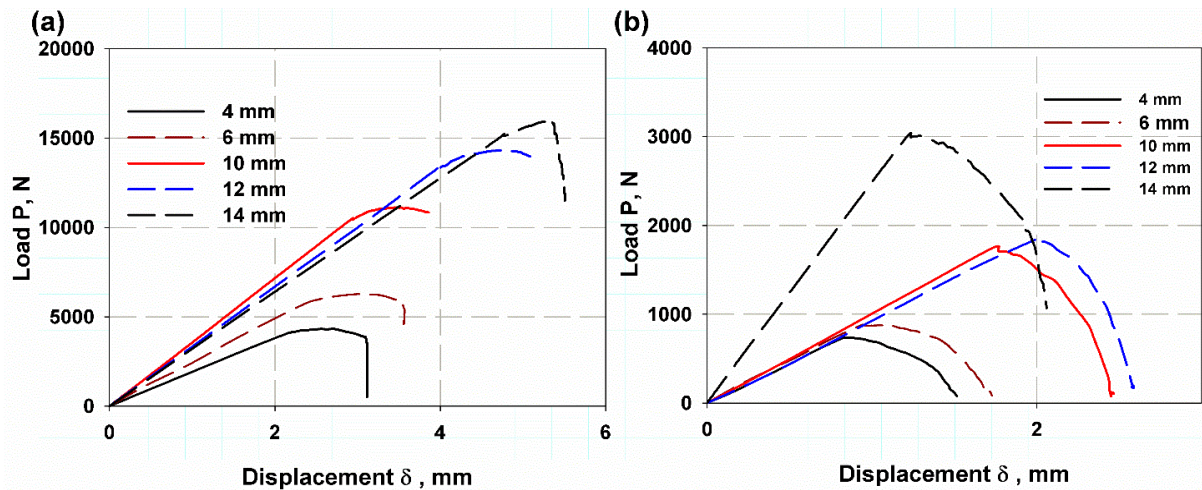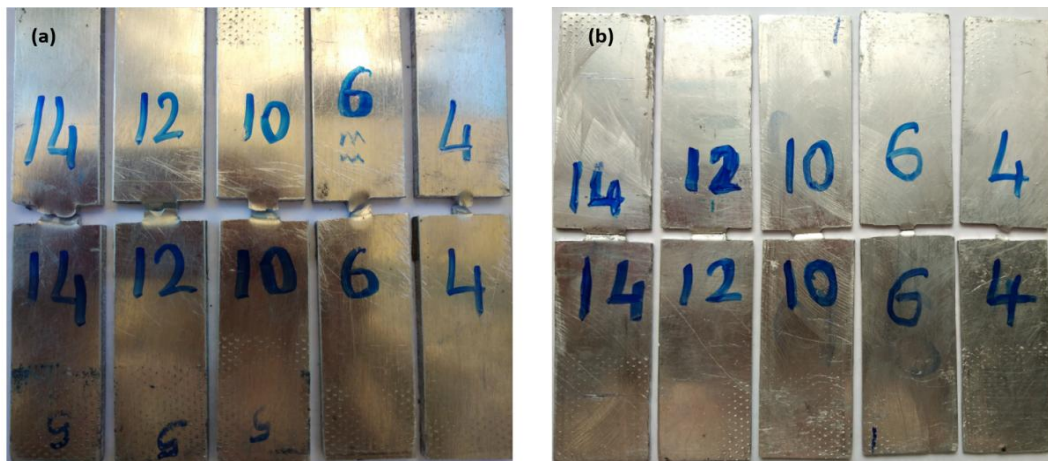

Figure 8. Load-displacement curve for DENT for (a) 5 mm thickness, (b) 1.8 mm thickness.
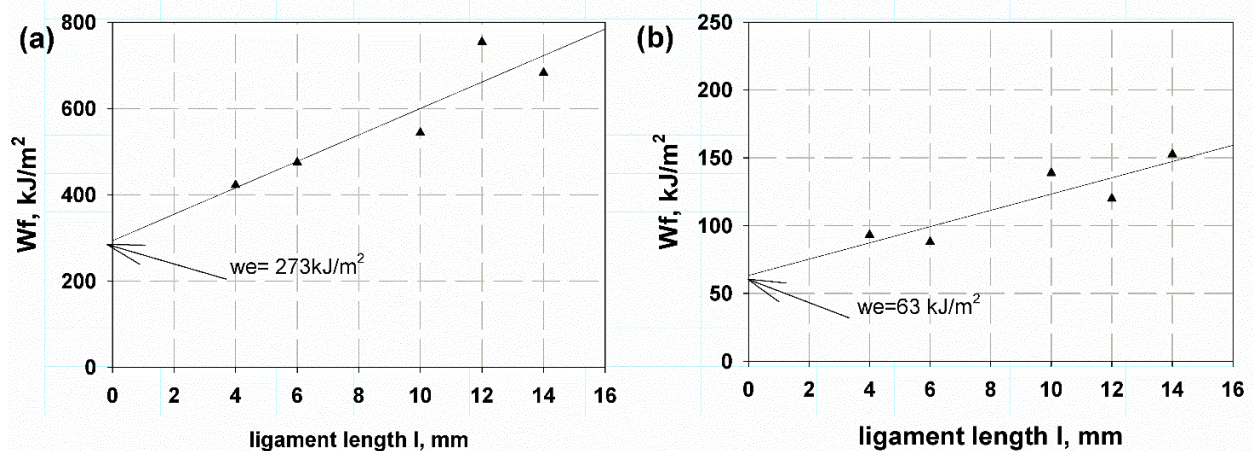
Figure 9. EWF fitting for DENT for (a) 5 mm thickness, (b) 1.8 mm thickness.
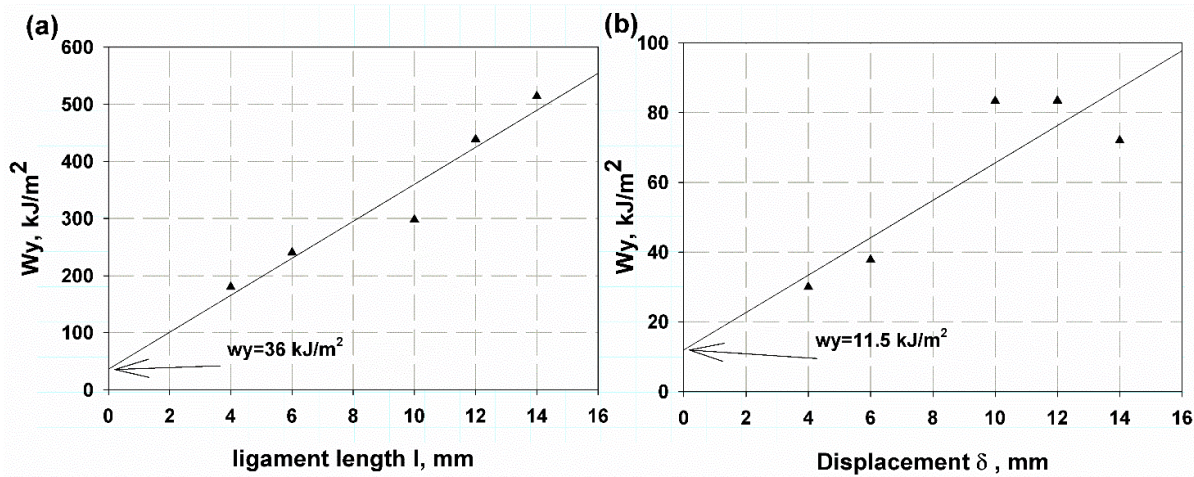
Figure 10. EWF data of elastic energy Wy for DENT for (a) 5 mm thickness, (b) 1.8 mm thickness.

Figure 11. Modes of failure for DENT for (a) 5 mm thickness, (b) 1.8 mm thickness.

4.3. Compact tension test

Figure 12a,b shows the curve of loading and displacement of the crack mouth. It was observed that for a 5 mm-thick slab (Figure 12a), the curve attains a mixing maximum and then, gradually decreases as the crack propagates. Meanwhile, for a thin slab with a thickness of 1.8 mm, it yields a flat plateau after attaining the maximum value. Figure 13a,b shows the crack propagation proceeding in a straight line with an undulating pattern owing to the plastic deformation by the crack surfaces.

The fracture toughness values (K_{IC}) were calculated from the peak load values (MPa$\sqrt{m}$) using Eq 12. According to the ASTM E399 standard, the critical stress intensity factor for the breaking load (p_Q) is given by [44]

$$K_{IC} = \frac{p_Q}{t\sqrt{W}}\, f\left(\frac{a}{W}\right)$$ (12)

where (t) is the specimen thickness, mm; (W) is the specimen width, mm; (a) is the crack length, mm; (p_Q) is the load at 5% secant; and $f\left(\frac{a}{W}\right)$ is the shape correction factor (see Eq 13):

$$f(a/w) = \frac{2 + a/w}{(1 - a/w)^{1.5}} [0.886 + 4.64(a/w) - 13.32(a/w)^2 + 14.72(a/w)^3 - 5.6(a/w)^4 \quad (13)$$

The critical strain energy release rate J_{IC} can be measured using Eq 14:

$$J_{IC} = \frac{K_{IC}{}^2}{E} \quad (14)$$

where E is the elastic modulus. Value of the energy release rate, J_{IC}, when the crack propagates (referred to as unstable crack growth). For materials and loaded configurations with an increasing resistance curve (or R-curve), J_{IC} is not unique. Examples of increasing and flat R curves are shown in Figure 12. With an increasing R-curve, the J_{IC} value is generally defined for crack initiation (assuming that a marginal amount of stable cracking occurs before unstable crack growth). This is analogous to the 0.2% proof stress derived from tensile tests on materials that do not have a distinct yield point (see Table 3).

The shape of the R-curve was influenced significantly by the size and geometry of the component. The R-curve resulting from a crack in a thin sheet is generally steeper than that resulting from a crack in a thick sheet. This is because a thin sheet is generally loaded in the plane, whereas the material at the crack tip of a thick sheet is under stress and is simultaneously loaded in the plane. The J_{IC} values were 34.5 kJ/m^2 and 10.6 kJ/m^2 for the specimens with thickness of 5 mm and 1.8 mm, respectively. The failure modes are illustrated in Figure 13. It was evidently a simple tension mode for the 5 mm-thick plate as shown in Figure 13-a. Here, there was a small bending through the specimen with the smaller thickness (1.8 mm) (see Figure 13-b).
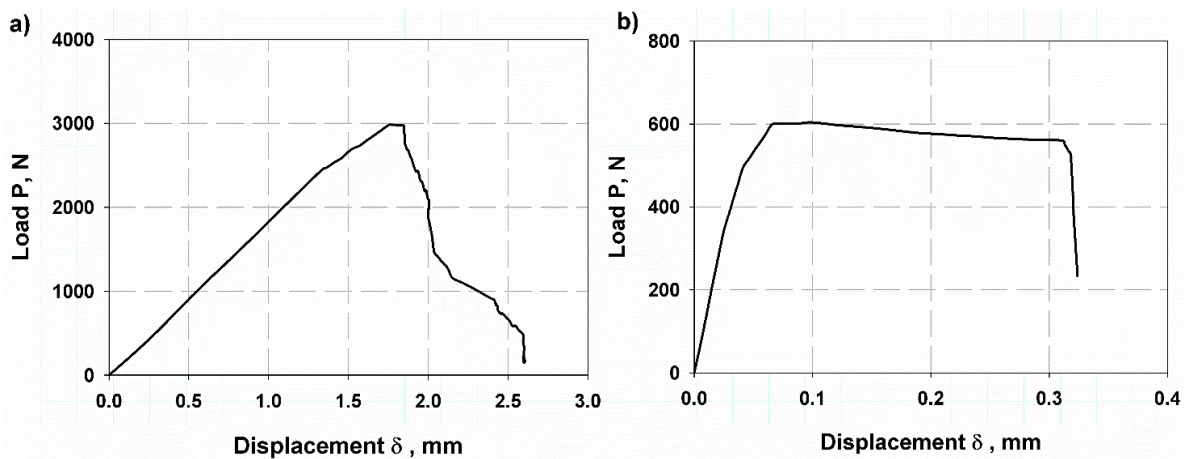
Figure 12. Load-displacement curve of CT specimens of (a) 5 mm thickness (b) 1.8 mm thickness.

Table 3. Fracture toughness corresponding to thickness.

Thickness (t, mm)	Crack length (a, mm)	p_Q (N)	K_{IC} (MPa$\sqrt{m}$)	J_{IC} (kJ/m^2)
5	34	3000	48.3	34.5
1.8	34	600	26.88	10.6
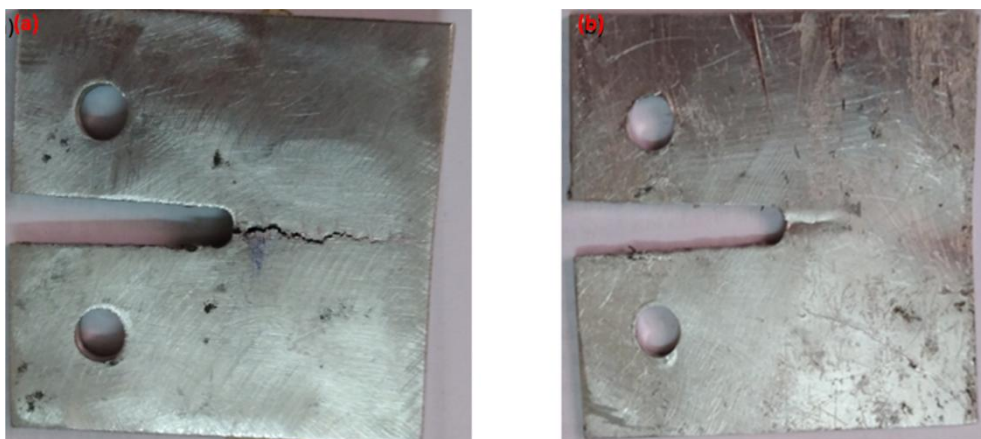
Figure 13. Modes of failure of CT test for thin-plate aluminium specimens: (a) 5 mm thickness (b) 1.8 mm thickness.

4.4. Comparison between methods

It was observed that the values of the elastic EWF wy were close to the release energy of the surface CT (see Table 4). The percentage variation was 5.8% in the case of the specimens with a thickness of 5 mm, whereas it was 8.4% for the 1.8 mm-thick slabs. This was because the CT indicates the fracture toughness at the beginning of the failure or at the beginning of the peak load based on a small plastic zone before the crack tip. This concept was developed using an elastic EWF. The elastic blow behaviour is characterised by a larger plastic deformation in front of the crack tip. Consequently, a linear fraction of elastic deformation exists in addition to the energy stored by the plastic deformation. Kobayshi and Yamada [45] determined the fracture toughness of a ductile damaged metal by correlating the average values of the initial and failure fracture toughness values over the entire R-curve. Test methods with different thicknesses yield different values. This is a generally debatable concept of fracture toughness measurement recommended by the ASTM standards [46]. The ASTM provides many methods for testing the fracture toughness of metals. Linear-elastic fracture mechanics refers to the fracture toughness of linear or elastic materials, whereas elastic–plastic fracture toughness (EPFM) refers to non-linear materials or materials with large plastic deformation (such as metals). The percentage error produced by the various methods was within a reasonable range from an engineer's perspective. In addition, the EWF method, which is based on the energy stored throughout the entire body, uses a different measurement criterion that does not depend on the LEFM and J-integral concepts. It rather depends on the strip length and the total work and energy stored in a cracked specimen [47,48] according to the EPFM [49]. It should be acknowledged that the EWF *(we)* considers the crack initiation resistance (G_{IC}). If the variation in (G_{IC}) is marginal [50], the relationship between the EWF *(we)* and J-integral (J_i) is valid according to the EPFM [51]. However, EWF is characterised by its simplicity of data reduction, sample preparation, and evaluation. This makes it attractive for measuring the fracture toughness of ductile thin films [52,54].

Table 4. Comparison between EWF and CT.

Specimen	Surface release energy J_{IC}, kJ/m^2		% of variation
	EWF	CT	
5 mm	36	34.5	5.8
1.8 mm	11.5	10.6	8.4

5. Conclusions

The mechanical and fracture properties of a structural material (the aluminium alloy 5754-H11) were determined. It was observed that the concept of essential work of fracture (EWF) was reasonable for measuring the surface energy in the case of elastic–plastic fracture mechanics J_{IC}. The EWF was affected by the sheet thickness. It was 273 kJ/m^2 for the specimens with a thickness of 5 mm, and 63 kJ/m^2 for the specimens with a thickness of 1.8 mm. These values represent the total fracture toughness of the plastic flow of ductile fracture materials (essential (elastic) and non-essential (plastic) fracture work). Therefore, the elastic work of fracture Wy could be determined as the area under the elastic zone of the load-displacement curves. Thus, the elastic EWF wy was 36 kJ/m²and 11.5 kJ/m^2 for the specimens with thicknesses of 5 mm and 1.8 mm, respectively. These two values of elastic work of fracture are close to the values obtained with the conventional standard specimen CT. Here, the surface release energies J_{IC} were 34.5 kJ/m^2 and 10.6 kJ/m^2 for the specimens with thicknesses of 5 mm and 1.8 mm, respectively. These values correspond to percentage errors of 5.8% and 8.4%, respectively, compared with the elastic EWF data. The large amount of Mg in the aluminium alloy 5754 was the main reason for the material embrittlement. It reduced the fracture toughness in the lower thickness. Meanwhile, the elements with Si formed a solid particle through the crack surfaces when these reacted with oxygen. It functioned as a bridge and thereby, reduced the crack propagation or crack propagation and then reinforced the fracture.

Acknowledgments

Conflict of interest

The authors declare no conflict of interest.

References

1. Fuller CB, Krause AR, Dunand DC, et al. (2002) Microstructure and mechanical properties of a 5754 aluminum alloy modified by Sc and Zr additions. *Mater Sci Eng A-Struct* 338: 8–16. https://doi.org/10.1016/S0921-5093(02)00056-4
2. Vetrano JS, Bruemmer SM, Pawlowski LM, et al. (1997) Influence of the particle size on recrystallization and grain growth in Al–Mg-X alloys. *Mater Sci Eng A-Struct* 238: 101–107. https://doi.org/10.1016/S0921-5093(97)00445-0

3. Abdellah MY (2021) Ductile fracture and S-N curve simulation of a 7075-T6 Aluminum alloy under static and constant low-cycle fatigue. *JFAP* 21: 1476–1488. https://doi.org/10.1007/s11668-021-01202-x

4. Cotterell B, Reddel J (1997) The essential work of plane stress ductile fracture. *Int J Fracture* 13: 267–277. https://doi.org/10.1007/BF00040143

5. Shinde PS, Singh KK, Tripathi VK, et al. (2012) Fracture toughness of thin aluminum sheets using modified single edge notch specimen. *IJEIT* 1: 283–288.

6. Tippeswamy M, Arun K, Naik S (2022) Investigations on fracture characteristics of Aluminium 6082-T6 alloy by using single edge notch bending. *IOP Conf Ser-Mater Sci Eng* 1258: 012038. https://doi.org/10.1088/1757-899X/1258/1/012038

7. Pardoen T, Hutchinson J (2000) An extended model for void growth and coalescence. *J Mech Phys Solids* 48: 2467–2512. https://doi.org/10.1016/S0022-5096(00)00019-3

8. Moiseenko DD, Maksimov PV, Panin SV, et al. (2020) Recrystallization at crack surfaces as a specific fracture mechanism at elevated temperatures-Cellular automata simulation. *Phys Mesomech* 23: 1–12. https://doi.org/10.1134/S1029959920010014

9. Balokhonov R, Romanova V, Batukhtina E, et al. (2016) A mesomechanical analysis of the stress-strain localisation in friction stir welds of polycrystalline aluminium alloys. Meccanica 51: 319-328. https://doi.org/10.1007/s11012-015-0250-9

10. alokhonov RR, Zinovyev AV, Romanova VA, et al. (2016) Numerical simulation of deformation and fracture of a material with a polysilazane-based coating. *Phys Mesomech* 19: 430-440. https://doi.org/10.1134/S1029959916040093

11. Abdellah MY (2017) Essential work of fracture assessment for thin aluminium strips using finite element analysis. *Eng Fract Mech* 179: 190–202. https://doi.org/10.1016/j.engfracmech.2017.04.042

12. Broberg K (1968) Critical review of some theories in fracture mechanics. *Int J Fracture Mech* 4: 11–19. https://doi.org/10.1007/BF00189139

13. Korsunsky AM, Kim K (2005) Determination of essential work of necking and tearing from a single tensile test. *Int J Fracture* 132: 37–44. https://doi.org/10.1007/s10704-005-4483-9

14. ASTM International (2001) Standard test method for measurement of fracture toughness[1]. E1820-01.

15. Tada H, Paris PC, Irwin GR (1973) *The Stress Analysis of Cracks Handbook*, 3 Eds., ASME Press.

16. Murakami Y, Keer L (1993) *Stress Intensity Factors Handbook*. https://doi.org/10.1115/1.2900983

17. Masuda K, Ishihara S, Oguma N (2021) Effect of specimen thickness and stress intensity factor range on plasticity-induced fatigue crack closure in a 7075-t6 alloy. *Materials* 14: 664. https://doi.org/10.3390/ma14030664

18. ASTM International (2011) Standard test method for measurement of fracture toughness. ASTM E1820-11.

19. Davey K, Zhang J, Darvizeh R (2022) Fracture mechanics: A two-experiment theory. *Eng Fract Mech* 271: 108618. https://doi.org/10.1016/j.engfracmech.2022.108618

20. Byskov E (1970) The calculation of stress intensity factors using the finite element method with cracked elements. *Int J Fract Mech* 6: 159–167. https://doi.org/10.1007/BF00189823

21. Lu L, Wang S (2017) Relationship between crack growth resistance curves and critical CTOA. *Eng Fract Mech* 173: 146–156. https://doi.org/10.1016/j.engfracmech.2016.12.010

22. Di Y, Shuai J, Wang J, et al. (2015) A new specimen for high-grade pipeline steels CTOA test. *Eng Fract Mech* 148: 203–212. https://doi.org/10.1016/j.engfracmech.2015.06.088

23. Kuno T, Yamagishi Y, Kawamura T, et al. (2008) Deformation mechanism under essential work of fracture process in polycyclo-olefin materials. *Express Polym Lett* 2: 404–412. https://doi.org/10.3144/expresspolymlett.2008.49

24. Abdellah MY, Zuwawi AR, Azam SA, et al. (2022) A comparative study to evaluate the essential work of fracture to measure the fracture toughness of quasi-brittle material. *Materials* 15: 4514. https://doi.org/10.3390/ma15134514

25. Hassan MK, Abdellah MY, ElAbiadi TS, et al. (2017) Essential work of fracture and size effect in copper/glass-reinforced epoxy laminate composites used as MEMS devices. *Am J Mech Eng* 5: 234–238. https://doi.org/10.12691/ajme-5-5-7

26. Demiray Y, Kavaklioglu Z, Yucel O (2015) A study on thermo-mechanical behavior of AA5754 alloy (tread and plain sheet) produced by twin-roll casting. *Acta Physica Polonica A* 127: 1097–1099. https://doi.org/10.12693/APhysPolA.127.1097

27. Rodríguez-Millán M, Vaz-Romero A, Rusinek A, et al. (2014) Experimental study on the perforation process of 5754-H111 and 6082-T6 aluminium plates subjected to normal impact by conical, hemispherical and blunt projectiles. *Exp Mech* 54: 729–742. https://doi.org/10.1007/s11340-013-9829-z

28. Abdellah MY, Alharthi H, Husein E, et al. (2021) Finite element analysis of vibration modes in notched aluminum plate. *JMERD* 44: 343–353.

29. ASTM International (2022) Standard Test Method for Linear-Elastic Plane-Strain Fracture Toughness of Metallic Materials. ASTM E399-22.

30. 100kN Computerized Universal Testing Machine. Available from: http://www.victorytest.com/products/wdw-50100-computerized-electromechanical-universal-testing-machine/.

31. ASTM International (2007) Standard test methods for plane-strain fracture toughness and strain energy release rate of plastic materials. ASTM D5045-99.

32. Abdellah MY, Alfattani R, Alnaser IA, et al. (2021) Stress distribution and fracture toughness of underground reinforced plastic pipe composite. *Polymers* 13: 2194. https://doi.org/10.3390/polym13132194

33. Abdellah MY, Sadek MG, Alharthi H, et al. (2023) Mechanical, thermal, and acoustic properties of natural fibre-reinforced polyester. *P I Mech Eng-J Pro* 09544089231157638. https://doi.org/10.1177/09544089231157638

34. Yilmaz S, Yilmaz T, Kahraman B (2014) Essential work of fracture analysis of short glass fiber and/or calcite reinforced ABS/PA6 composites. *Polym Eng Sci* 54: 540–550. https://doi.org/10.1002/pen.23584

35. Mai YW, Cotterell B (1986) On the essential work of ductile fracture in polymers. *Int J Fracture* 32: 105–125. https://doi.org/10.1007/BF00019787

36. Yilmaz S, Yilmaz T, Armagan Arici A (2011) Effect of annealing process in water on the essential work of fracture response of ultra high molecular weight polyethylene. *J Mater Sci* 46: 1758–1766. https://doi.org/10.1007/s10853-010-4996-0

37. Hashemi S (2003) Work of fracture of high impact polystyrene (HIPS) film under plane stress conditions. *J Mater Sci* 38: 3055–3062. https://doi.org/10.1023/A:1024752508458

38. Andriescu A, Hesp SA, Youtcheff JS (2004) Essential and plastic works of ductile fracture in asphalt binders. *Transport Res Rec* 1875: 1–7. https://doi.org/10.3141/1875-01

39. Caracostas CA, Chiou WA, Fine ME, et al. (1997) Tribological properties of aluminum alloy matrix TiB$_2$ composite prepared by in situ processing. *Metal Mater Trans A* 28: 491–502. https://doi.org/10.1007/s11661-997-0150-2

40. Allison JE, Cole GS (1993) Metal-matrix composites in the automotive industry: opportunities and challenges. *JOM* 45: 19–24. https://doi.org/10.1007/BF03223361

41. Dhingra AK, Fishman SG (1986) *Interfaces in Metal-Matrix Composites*, Warrendale, PA: Metallurgical Society, Inc.

42. Abdellah MY, Fadhl BM, Abu El-Ainin HM, et al. (2023) Experimental evaluation of mechanical and tribological properties of segregated Al–Mg–Si alloy filled with alumina and silicon carbide through different types of casting molds metals. *Metals* 13: 316. https://doi.org/10.3390/met13020316

43. Anderson K, Kaufman JG, Weritz J (2019) *ASM Handbook: Volume 2B Properties and Selection of Aluminum Alloys*, The Netherlands: ASM International Almere. https://doi.org/10.31399/asm.hb.v02b.9781627082105

44. Mohammed Y, Hassan MK, El-Ainin HA, et al. (2014) Effect of stacking sequence and geometric scaling on the brittleness number of glass fiber composite laminate with stress raiser. *Sci Eng Compos Mater* 21: 281–288. https://doi.org/10.1515/secm-2013-0038

45. Kobayash T, Yamada S (1994) Evaluation of static and dynamic fracture toughness in ductile cast iron. *Metal Mater Trans A* 25: 2427–2436. https://doi.org/10.1007/BF02648862

46. Anderson TL (2017) *Fracture Mechanics: Fundamentals and Applications, CRC press*. https://doi.org/10.1201/9781315370293

47. Williams J, Rink M (2007) The standardisation of the EWF test. *Eng Fract Mech* 74: 1009–1017. https://doi.org/10.1016/j.engfracmech.2006.12.017

48. Cotterell B, Reddel J (1977) The essential work of plane stress ductile fracture. *Int J Fracture* 13: 267–277. https://doi.org/10.1007/BF00040143

49. Rice JR (1968) A path independent integral and the approximate analysis of strain concentration by notches and cracks. *J Appl Mech* 35: 379–386. https://doi.org/10.1115/1.3601206

50. Cotterell B, Atkins A (1996) A review of the J and I integrals and their implications for crack growth resistance and toughness in ductile fracture. *Int J Fracture* 81: 357–372. https://doi.org/10.1007/BF00012428

51. Mai YW, Powell P (1991) Essential work of fracture and j-integral measurements for ductile polymers. *J Polymer Sci Pol Phys* 29: 785–793. https://doi.org/10.1002/polb.1991.090290702

52. Gobbi G, Colombo C, Vergani L (2016) Sensitivity analysis of a 2D cohesive model for hydrogen embrittlement of AISI 4130. *Eng Fract Mech* 167: 101–111. https://doi.org/10.1016/j.engfracmech.2016.03.045

53. Barany T, Czigány T, Karger-Kocsis J (2010) Application of the essential work of fracture (EWF) concept for polymers, related blends and composites: A review. *Prog Polym Sci* 35: 1257–1287. https://doi.org/10.1016/j.progpolymsci.2010.07.001

54. Heidari F, Aghalari M, Tehran AC, et al. (2021) Study on the fluidity, mechanical and fracture behavior of ABS/TPU/CNT nanocomposites. *J Thermoplast Compos* 34: 1037–1051. https://doi.org/10.1177/0892705720978696